Arroyo, I. H., Rezgui, D., & Theunissen, R. (2016). Analytical Model for Leading-Edge Vortex Lift on Rotating Samara Seeds: Development and Validation. In Proceedings of Applied Aerodynamics Conference 2016: Evolution and Innovation Continues - The Next 150 Years of Concepts, Design and Operations. (2016 Applied Aerodynamics Conference). The Royal Aeronautical Society.

ANALYTICAL MODEL FOR LEADING-EDGE VORTEX LIFT ON ROTATING SAMARA SEEDS: DEVELOPMENT AND VALIDATION

Mr Ignacio Hernández Arroyo[1] Dr Djamel Rezgui[2] Dr Raf Theunissen[3]

Department of Aerospace Engineering, University of Bristol, Queen's Building, University Walk, Bristol. BS8 1TR. UK.

I. ABSTRACT

This article focuses on the development of a simple analytical aerodynamic model capable of describing the effect of Leading-Edge Vortices (LEVs) on the lift of samara wings. This was based on an adaptation of Polhamus' method to predict the lift function implemented in a numerical blade-element model for a rotating Samara blade. Furthermore, wind tunnel experiments were conducted to validate the numerical blade element model. The final results showed very good agreement between the developed numerical model and the experimental measurements in the prediction of samara wing rotational speed and rate of descent. This research furthered the understanding of the aerodynamic behaviour and modelling of LEVs on samara seeds for performance-prediction and could ultimately be used in the design of rotary micro-air vehicles.

Keywords: Aerodynamic model, Wind tunnel, Samara, Sycamore seed, Leading Edge Vortex, LEV.

II. INTRODUCTION

Samara seeds are a type of seed that has a fibrous wing allowing it to rotate to reduce their falling speed (figure 1). This in turn enables the see to be pushed further away from the parent tree for germination [1].

These seeds have been known to have very high sectional lift coefficients due to the development of what is known as a Leading Edge Vortex (LEV) over the wing (Figure 2) [2].

Figure 1: *Rotating samara seed recorded during the experiments of this research.*

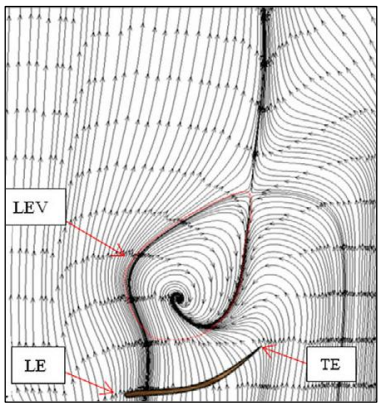

Figure 2: *Samara LEV sectional streamlines from Salcedo's Stereoscopic Particle Image Velocimetry experiments* [3].

The LEV is a phenomenon whereby a vortex is being developed along the wing from its leading edge. This LEV is an example of intricate flow mechanisms found to occur on natural wings such as in birds [1] [2], insects [3], bats [4], samara seeds [8][6][7], and also on artificial delta wings [5].

[1] Graduate Student, email: ih12315.2012@my.bristol.ac.uk

[2] Lecturer in Aerospace Engineering (corresponding author), email: djamel.rezgui@bristol.ac.uk

[3] Lecturer in Aerodynamics, email: r.theunissen@bristol.ac.uk

Animals use flapping in order to generate and sustain LEVs that lead to lower pressure (suction) and greater lift in the wing [4] [5]. It has also been suggested that a spanwise flow along the vortex core may be responsible for maintaining the stability of the LEVs [4]. Furthermore, insects seem to control their lift-enhancing vortices primarily through the mechanism of dynamic stall, unlike samara seeds [6]. Certain control of the creation of LEVs has been seen in bats depending on their flight regime. For manoeuvring and slow flight the increase in lift is useful, while the increase in drag also caused by the LEV is not an issue due to the lower speeds. However, this is not so in cruise speed, and therefore the bats are able to negate the creation of LEVs [7].

Interestingly, such LEVs have also been observed in low aspect ratio (AR) delta wings. It has been found that the sweep angle is directly related with the relative contribution of vortex lift. Nonetheless, increased sweep angle also diminishes the angle of attack at which the vortices detach [8].

Several experimental studies of samara LEVs have been performed successfully, obtaining good results and advancing the understanding in the topic. In 2009, Lentink explained how different species of samara seeds use LEVs to improve their lift-generating characteristics during autorotation (self-spinning) [2]. He also noted how more compact LEVs (due to decreasing angles of attack) and strong spanwise flows on the top of the aerofoil contributed to the attachment of the vortices and to better aerodynamic performance.

Salcedo confirmed later the importance of strong spanwise flow and strain produced by centrifugal forces in order to stabilise and attach the LEVs [3]. The attached LEVs create a straight cone pattern that augments lift generation, and the spanwise flow stretches and adds intensity to the LEV, preventing its detachment.

Yasuda and Azuma [9] on the other hand, concluded that the negative camber near to the root, the pattern (surface roughness) of the fibrous wing, and the leading edge extra thickness close to the root lead to the enhanced aerodynamic characteristics observed in samara seeds, suggesting that they may play a key role in the stability of LEVs.

Despite these studies, the lack of a theoretical model that tries to explain the flight of samara seeds (even in a limited fashion) is quite remarkable.

In Ansari *et al*.' review on aerodynamic modelling of insect-like flapping flight [10], several steady, quasi-steady, and unsteady methods used to create different models were discussed, including techniques capable of modelling LEVs for insect flight and delta wings. It is expected that these theories can be extended to samara wings. In particular, a promising method was implemented inside Traub's semi-empirical model (quasi-steady model with empirical corrections) in order to compute the effect of LEVs. This was Polhamus' leading-edge suction analogy [11], and it was originally developed for delta wings, but it was also used successfully in models for insect flight [12][13] and lift generation of avian tails [14], among others.

In this paper the authors present an adaptation of Polhamus' method was into an analytical model capable of describing the lift function for samara seeds autorotating flight. The model has been assessed against experimental wind tunnel data. The use of the method and the assumptions inherent to it will be justified, and the experimental adjustments and validation are also analysed.

III. METHODOLOGY

The analysis presented in this article is composed of three main elements:

1) Analytical development of an expression for lift coefficient of a rotating aerofoil with LEV.
2) Performance analysis of rotating samara wing in autorotation in vertical flight conditions using simple blade element method.
3) Wind tunnel testing of rotating samara seeds with the purpose of validating the numerical analysis.

1. Analytical model description

Polhamus' model [10] is based on an analysis of the wing using lifting surface methods to extract constants capable of describing the effect of the LEV on the total lift. It assumes that if the LEV remains attached over the upper surface of the wing the total lift will be obtained as the sum of the potential lift and a vortex lift.

This vortex lift will be related to the suction force on the leading edge, translated as a normal force on the upper surface of the aerofoil by imposing a Kutta flow condition at the leading edge (Figure 3).

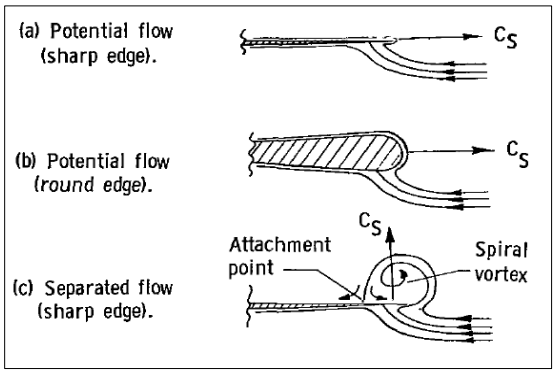

Figure 3: *Image of the leading-edge flow conditions from Polhamus method* [11].

The magnitude of the normal force at any wing section will be the suction created by the centrifugal force of the vortex lift. This can be seen expressed by potential flow and vortex lift components, in the following formulae (derived from Polhamus' paper [10]):

Potential flow lift component:

$$C_{L,p} = K_p sin \propto cos^2 \propto \qquad (1)$$

where $\propto$ is the local angle of attack (AoA).

This potential flow lift coefficient $C_{L,p}$ for small angles of attack will be reduced to:

$$C_{L,p} \approx K_p \propto = \frac{\delta C_L}{\delta \propto} \propto \qquad (2)$$

Therefore K_p will be given by the C_L (lift coefficient) over $\propto$ curve of small-angle theory, and will be derived from any adequate lifting-surface theory. In this case, the Vortex Lattice Method (VLM) code Tornado was used [15], in which a wing with AR = 4.38 and aerofoil NACA 0005 was analysed (Figure 4) and the variation of C_L over AoA was obtained using a 2nd order gradient scheme.

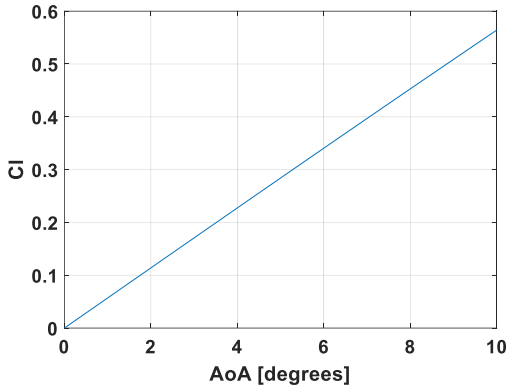

Figure 4: *Cl over Angle of Attack (AoA) line obtained from VLM Tornado.*

Vortex lift component:

The suction force will be rotated into the direction normal to the wing chord plane, and after the leading-edge thrust coefficient is determined, the vortex lift will be calculated:

$$C_{L,v} = K_v \frac{cos \propto}{cos\Lambda} sin^2 \propto \qquad (3)$$

Where Λ is the sweep angle and K_v is given by:

$$K_v = (K_p - {K_p}^2 K_i) \qquad (4)$$

And K_i will be equal to:

$$K_i = \frac{\delta C_{Di}}{\delta {C_L}^2} \qquad (5)$$

C_{Di} is the induced drag coefficient and C_L is the lift coefficient. It then follows that K_i can also be obtained using data from any reliable lifting-surface theory, such as VLM Tornado [15].

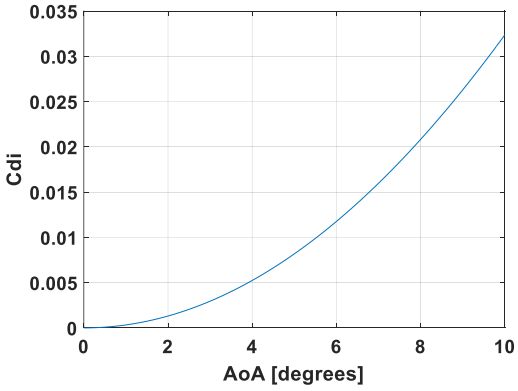

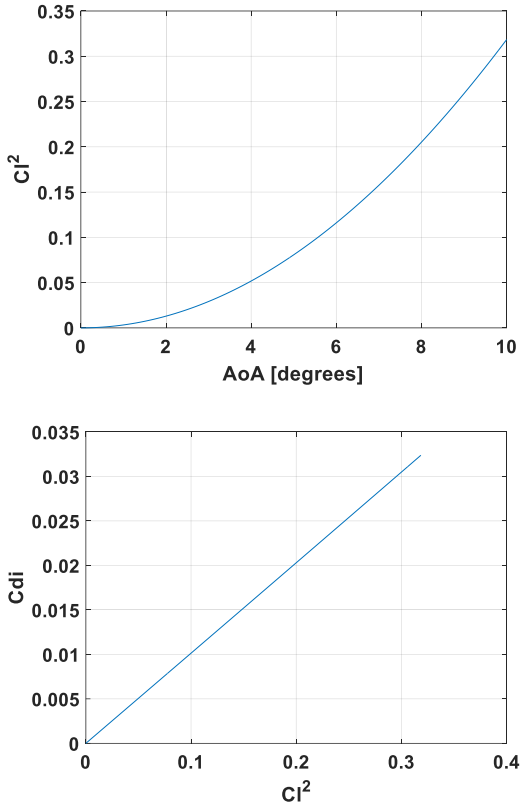

Figure 5: *Variation of C_{Di}* ***(top)*** *and $C_L{}^2$* ***(middle)*** *with respect to angle of attack (AoA) from the VLM Tornado data, and plot of C_{Di} versus $C_L{}^2$* ***(bottom)****.*

K_i was extracted using a 2nd order gradient scheme on the data set shown in the bottom graph of Figure 5.

The total lift is then given as the combination of the potential flow lift and the vortex lift:

$$C_L = C_{L,p} + C_{L,v}\,;$$

Hence:

$$C_L = K_p sin \propto cos^2 \propto$$

$$+ (K_p - K_p{}^2 * K_i)\frac{cos \propto}{cos\Lambda} sin^2 \propto \qquad (6)$$

2. Performance validation using Blade element methods

Data for the simplified samara wing was obtained from the lifting-surface method VLM (Vortex Lattice Method) Tornado [15] and checked against the analysis of the same wing in AVL [16] (see Figure 6). This check was carried out to ensure the data being used for the model was sensible, as using wildly inaccurate data would have led to an unusable model.

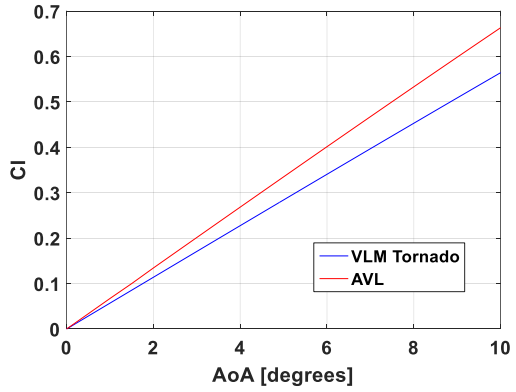

Figure 6: *Cl vs AoA (Angle of Attack) curves obtained from VLM Tornado (wing with AR=4.38 and NACA 0005 aerofoil) and AVL (wing with AR=4.38 and NACA 0005 aerofoil).*

The samara wing analysed in the lifting surface methods was simplified as a rectangular wing, with no sweep. The aspect ratio (AR) equalled 4.38, and an aerofoil NACA 0005 (see Figure 7) was selected as it has no camber, low thickness, and a leading edge with low radius of curvature, resembling the cross section of the samara seed. The data was then used to obtain the required constants for Polhamus' LEV lift, as discussed in Section III.1.

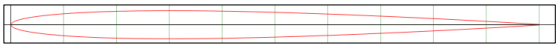

Figure 7: *NACA 0005 aerofoil used in VLM Tornado and AVL.*

The justification for the use of Polhamus method for our wing comes from the extensions of Polhamus method. In Lamar's application of the method for rectangular wings [17] he showed how a side edge suction force would exist for this kind of wings, analogous to the leading-edge suction force shown in Figure 3. It is explained how the vortex lift coming from the side edge suction will tend to 0 as AR tends to infinity, and in the data from Lamar published by Bradley [18] it can be seen how this side vortex lift reduces very steeply from AR=0.5 to AR=2, leading to the conclusion of being able to neglect the side edge vortex lift for our AR of 4.38. Furthermore, using an aerofoil with a non-sharp leading edge can be acceptable, as Lamar and Bradley stated how a thicker leading edge would simply delay the creation of LEVs [17]. Nevertheless, as this model assumes the LEV has already been created this should not affect the accuracy of the model.

Having checked the assumptions made in the model are acceptable, the first complete analysis with the lift model on samara seeds was obtained when the results from Polhamus' method were included in the Blade-Element Model (BEM), a numerical rotor model using strip theory with steady aerodynamics combined with momentum theory. The BEM was set up in MATLAB as a set of algebraic equations describing the seed equilibrium conditions in vertical autorotation descent. The equations returned the values for the rotational speed, rate of descent and induced velocity, for different varying blade properties, such as the blade disk loading or blade pitch angle. This model was tuned to fit Azuma's [19] experimental results for samara seeds.

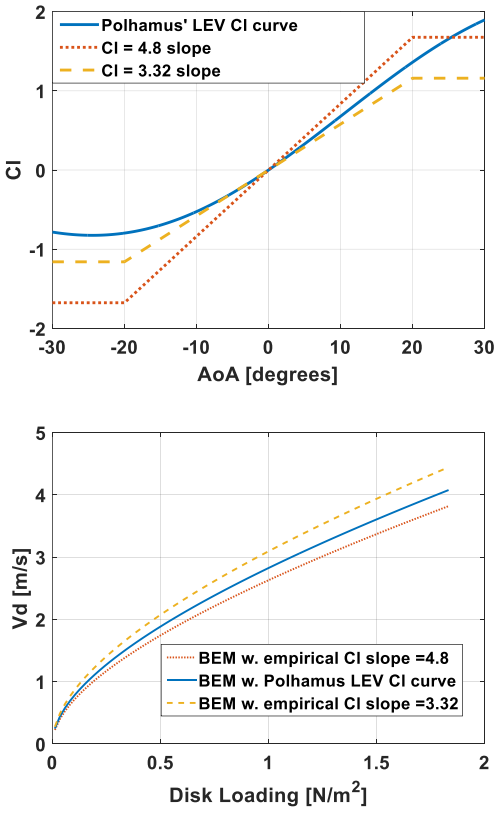

Figure 8: *Variation of the Samara seed vertical descent speed (Vd) with disk loading* ***(bottom)*** *for different lift coefficient functions* ***(top)****.*
The Cl curves were obtained from the experimental slopes from Azuma [19] *with a "stall" (plateau) at ±20º and the results from Polhamus' method, comparing the use of the maximal and minimal Cl values from experimental data* [19] *and the Cl from the LEV model. AR=4.38 used in all cases.*

The model using the analytical lift curve was compared against results with the empirical lift coefficient curves [19] (Figure 8). It can be seen that the results obtained from the analytical LEV model are sensible, falling between the range of the minimal and maximal experimental values [19].

3. Wind tunnel experiments:

To independently validate the results of the model, experiments in a vertical low speed wind tunnel were carried out. These experiments required the project to be divided in several stages, which are described in the following sections.

Experiments in previous literature

A number of experimental studies on the flight dynamics and aerodynamics of samara seeds have been reported in previous [2][3][20][21].

The studies were carefully analysed to obtain a good insight into the construction of the proper experimental setup for the purpose of the achieving the objectives of this validation study. This was concluded by designing and building a specific vertical low speed tunnel.

Design of the wind tunnel

The wind tunnel was designed to be modular, with each section manufactured separately and then assembled together. This was to make it possible for future modifications and improvements in the design. The material used tunnel was acrylic glass, due to easy availability and adequate material properties. Reinforcements were used at the corners to ensure the rigidly of the structure.

From basic wind tunnel design [22][23] several sections for the wind tunnel were determined, namely: working section, contraction, two wire mesh separations, honeycomb section, and fan section (or in this case, fan plate). In Figure 9, a basic schematic is shown, based on the CAD (Computer-Aided Design) drawings of the wind tunnel.

The working section was designed with internal dimensions of 340 mm x 340 mm, and a total length of 600 mm. The interior dimensions were selected in order to minimise interference of the walls of the working section with the flow inside the tunnel. The length of the working section was selected with guidance from the designs of previous wind tunnels used in the research mentioned previously, adding some

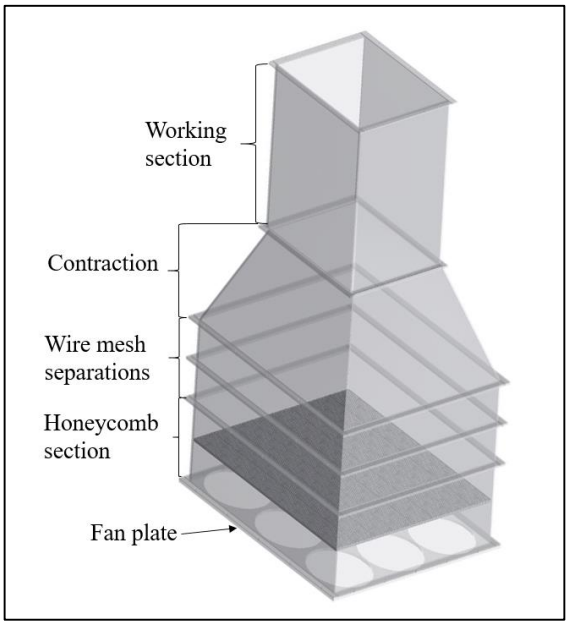

Figure 9: *Schematic of the designed low-speed vertical wind tunnel with its different modules.*

extra length (600 mm vs 500 mm used by Salcedo [3]) to have flexibility for future research.

The material of the working section was selected to be transparent acrylic glass, in order to facilitate the observation of the experiments and to allow to perform future Particle Image Velocimetry (PIV) experiments.

The contraction connects the wire mesh separations with the working section, changing from 600 mm x 590 mm to 340 mm x 340 mm. This gave an area ratio of 3.06.

According to previous research [23] area ratios lower than six risk leading to high pressure losses through the wire screens (wire meshes). Nonetheless, area ratios bigger than the present could not be achieved without either diminishing the area of the working section or increasing the area of preceding sections, which would have limited future experiments. Thus the present contraction design was selected.

The honeycomb was positioned 100 mm away from the fans, to allow for unobstructed flow intake and flow development from the fans, while leaving 180 mm before the first wire mesh, and as the selected honeycomb had a thickness of 20 mm, giving a total length of the honeycomb section of 300 mm.

The fan plate is attached to supports a total of nine fans to deliver the air flow into the wind tunnel. Given the size and budget of the project nine *BitFenix Spectre PRO (230 mm)* [24] were used for the wind tunnel. The fans were connected on a parallel circuit, and to a power source capable of regulating the voltage delivered to the circuit, which allowed for the wind speed to be modified.

Set up arrangement:

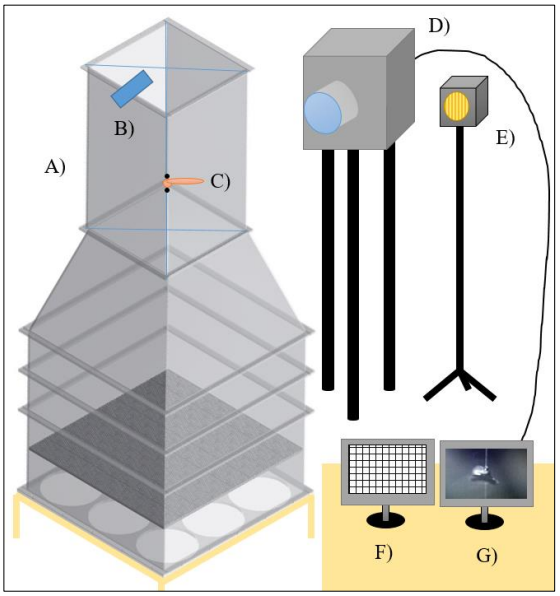

Figure 10: *Schematic of the final experimental set up, including:*
A) *Wind tunnel,* ***B)*** *anemometer for wind speed measurements,* ***C)*** *sample samara seed,* ***D)*** *high speed camera for rotation observation,* ***E)*** *LED spotlight,* ***F)*** *computer for measurements input,* ***G)*** *computer receiving high speed camera video.*

Several samples of sycamore seeds (*Acer Pseudoplatanus*) [25][26] were collected in autumn, and they were kept in a sealed container that was checked daily to ensure that the humidity was adequate for the preservation of the specimens (the container was ventilated or added humidity depending on the apparent dryness and structural integrity of the samples).

The criteria for selecting the seeds was the health of the seed, the span of the wing and the aspect ratio (as suggested by Azuma [9]). The final aspect ratio used was about 4.38.

Due to time constraints the two specimens that best fit the criteria were selected and prepared for the experiments. This involved calculating their centre of gravity position (CG), in order to find their natural centre of rotation.

At the approximate CG, a hole was drilled in the seed with a 0.5 mm straight needle, and then the

seed was set into the working section of the wind tunnel using 0.23 mm thin transparent fishing wire with knots to avoid the seed moving, and with 2 mm beads to minimise friction and possible jamming of the knots in the holes of the seeds.

Wind tunnel characterisation:

The wind tunnel characterisation is a process in which the quality of the airflow in the wind tunnel is checked, namely the level of turbulence, uniformity, and steadiness of the flow.

To carry out the characterisation processes, two anemometers and a mini-CTA (Constant Temperature Anemometer) probe [27] were used to perform wind speed measurements at the end of the contraction section (the point of connection between the contraction and the working section) and at the end of the working section (see figures 9, 10 and 12).

It is worth noting that the anemometers had a precision of 0.1 m/s, while the mini-CTA probe could measure variations of up to 0.001 m/s.

After checking the correct calibration of the probe, its measured wind speed was compared with the values from the anemometers. One of the anemometers was observed to output a wind speed 0.3-0.4 m/s higher than the measurements of the probe, while the second anemometer gave values that agreed with the CTA. The latter was selected for the wind speed measurements, as the mini-CTA probe was not available for the entirety of the experiments.

As the mini-CTA also allowed to record measurements during lapses of time, it was used to observe the steadiness of the flow at different voltage-current inputs of the wind tunnel. In Figure 11 b), it can be seen that the flow was steady for the 12 V setting, with small fluctuations in the Vd (vertical velocity). Whereas for the 3.9 V setting, the flow was much more unsteady, with changes in Vd of almost 0.5 m/s (Figure 11 a)). This was observed to take place because the current was not enough to power all the fans, and some of the fans of the wind tunnel were working intermittently, instead of continuously as for higher voltage settings.

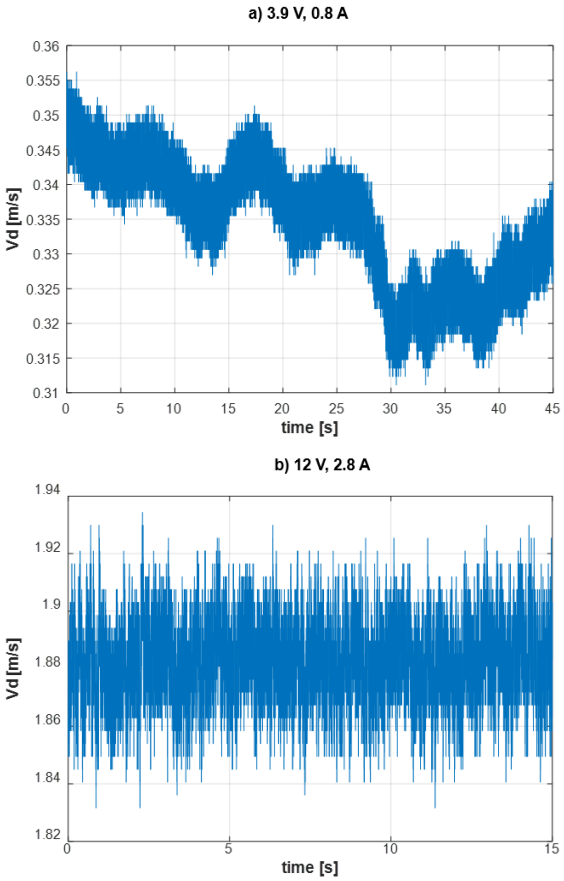

Figure 11: *Mini-CTA probe vertical flow speed measurements at the centre of the top end of the wind tunnel working section. 3.9 V measurements (10a,* ***top****) and 12 V measurements (10b,* ***bottom****).*

The highly unsteady and fluctuating flow was only observed for the 3.9 V setting, for all the tests performed at higher voltage inputs the flow was found to be almost steady as seen in Figure 11 b) for the 12 V input.

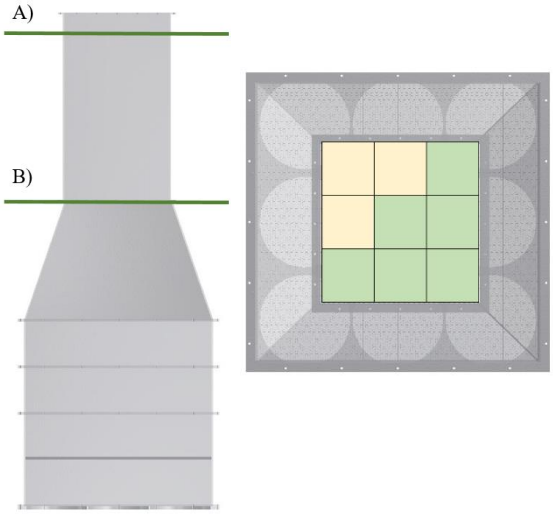

Figure 12: *Front* ***(left)*** *and top* ***(right)*** *view of the characterisation measurements.*

Left: *Horizontal planes of measurement for the wind tunnel characterisation:* ***A)*** *Plane at the end of the working section,* ***B)*** *plane at the connection between the contraction and the working section.*
Right: *Points of wind speed measurement on the horizontal measurement planes. Green cells show the wind speeds directly obtained by measurement, yellow cells show the ones calculated by symmetry.*

Having selected and calibrated the anemometer, measurements in the wind tunnel were performed to check for flow uniformity across the working section. As observed in Figure 12, they were performed in two sections (planes of measurement) of the wind tunnel: the end of the working section (plane (A) in Figure 12) and the connection between the contraction and the working section (plane (B) in Figure 12). The speed measurements were obtained at six points of each plane, which after taking into account the symmetry of the structure were translated into nine measurements (in Figure 12, right, the points directly measured are marked in green, the measurements calculated by symmetry are shown in yellow).

The measurements were taken at settings in which the flow was almost steady, in order to observe its uniformity, and therefore inputs above 3.9 V were observed, namely: 4 V, 7 V, 10 V and 13 V. The average and standard deviation of the values were calculated:

Table 1: *Vertical velocity (Vd) average (AVG) and standard deviation (σ) of the characterisation*

	Voltage (V)	**4**	**7**	**10**	**13**
Working section	AVG (m/s)	0.422	1.089	1.539	1.9
	σ (m/s)	0.024845	0.021	0.021	2.2E-16
Contraction	AVG (m/s)	0.47	1.1	1.594	1.9
	σ (m/s)	0.025	2.2 E-16	0.044	2.22E-16

From these measurements it could be concluded that for voltage settings above 3.9 V the wind tunnel produces an almost steady and uniform flow (see Vd standard deviation in Table 1, ranging from 0.04 to almost 0). The pressure losses due to the wire meshes, the honeycomb panel, and the contraction design are quite noticeable, giving a maximum flow velocity of 1.9 m/s, for the 13 V setting, while the ideal theoretical flow was

IV. EXPERIMENTAL MEASUREMENTS

With the final set up arranged and having characterised the wind tunnel, the experimental measurements for the analytical model validation were performed. This was done taking measurements of the rotational speed (omega) and vertical flow velocity (Vd).

The videos recorded by the high speed camera were used to calculate the rotational speed of the samara wing with a good precision, while the anemometer positioned at the end of the working section (Figure 12 A)) was used to obtain Vd. The measurements were taken twice (first changing the voltage from lowest to highest setting and then from highest to lowest) to reduce human error and to check for any of hysteresis behaviour.

The settings used were from 4 to 13 V with steps of 0.5 V between each one.

Each wind speed measurement was taken during 15 s to take into any short term changes in the initial value. It should be noted that even though the anemometer was only able to measure with a resolution of 0.1 m/s, measurements were repeated at the same voltage setting and then averaged to obtain a more accurate flow speed value. In particular, when the anemometer oscillated more than three times during the measurement period, it was assumed that the actual wind speed was the average of the measured maximum and minimum values (e.g. if the oscillation happened between 1.5 m/s and 1.6 m/s the final value was recorded as 1.55 m/s).

Figure 13 shows a plot of the measured rotational speed values against vertical flow speed (Vd) values. The line of best fit passing through the origin (0, 0) is also illustrated in red.

Furthermore, the high speed camera was used to measure the coning and pitch angles. It is worth noting that due to the nature of the experiments and the preparation of the samples (with the axis

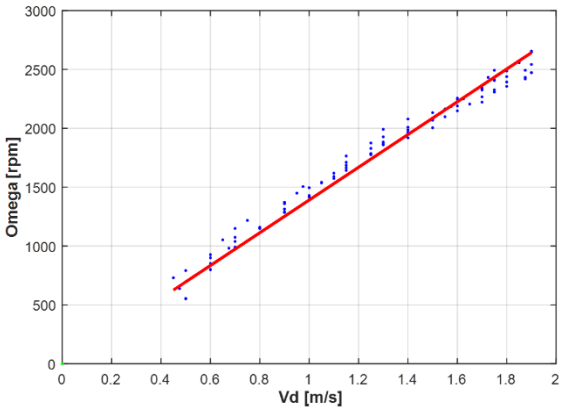

Figure 13: *Experimental data from all the rpm and vertical speed (Vd) measurements, with best fit line.*

of rotation drilled through the CG, and the fishing wire parallel to the air flow) the coning and pitch angles were quite restricted.

From the coning angle measurements (see examples in Figure 14), it was observed that the coning angle was close to 0 degrees. The pitch angle presented more difficulty being measured due to the natural twist of the blade; nevertheless, it was estimated to be between -5 and -7 degrees. The flapping rate of the seed was confirmed to be zero. These were important measurements in order to input them to the analytical BEM (with the LEV C_L curve).

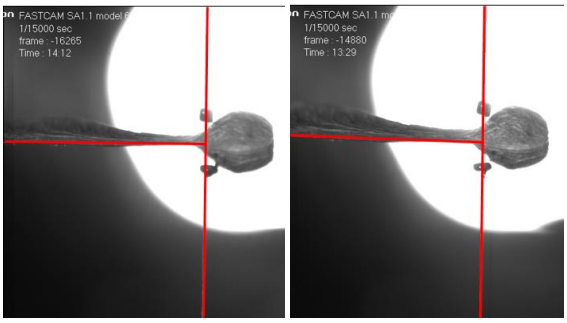

Figure 14: *Coning angle measurements at voltage 4 V (Vd≈0.5 m/s)* ***(left)*** *and 13 V (Vd≈1.9 m/s)* ***(right)***

V. MODEL VALIDATION

The model shown in the Methodology section (Sec. III.2) was updated with the values obtained from the experiments:

- Coning angle was set to 0 deg.
- Flapping rate was set to 0 rad/s.
- Pitch angle was varied from -5 deg to -7 deg., the best fit was selected (-7 deg).

The results from the Blade Element Model showed a great degree of agreement with the experimental results, with the best fit curve from the experimental results essentially overlapping the curve from the analytical LEV model (pitch angle = -7 deg in Figure 15). This is caused by the experimental results being tightly spread close to the prediction of the analytical model, confirming the hypothesis of the theoretical model matching the experimental results and leading to the validation of the analytical model for Leading-Edge Vortex lift on rotating samara seeds.

The experimental results were also compared against the other possible estimated pitch angles of -5 deg and -6 deg, see Figure 15.

Finally, the model with the tuned variables was run comparing with Cl curves from experimental data, shown in Figure 8 (top). The comparison can be seen in Figure 16. The results indicate yet another argument in favour of using the developed Polhamus' model to capture the lift effect due to the presence of the LEV of the samara seed. It can be clearly seen that the LEV model fits the experimental data better than the models where the empirical lift curve slopes from Azuma [19] were used.

In brief, it can be confirmed that an analytical model capable of predicting the lift on samara seeds with an active LEV has been developed, using an adaptation of Polhamus' method and a numerical blade element model. It has been checked against previous experimental data of lift curve slopes, and it has been validated experimentally.

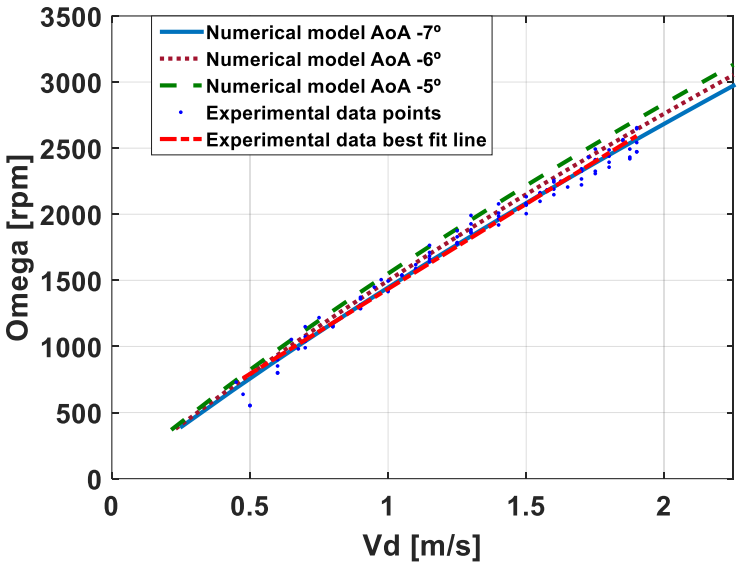

Figure 15: Tuned model results and experimental results (incl. best fit line), with a comparison of the changes on the BEM results when pitch angle was varied. Omega (rpm) = revolutions per minute, Vd = vertical flow speed.

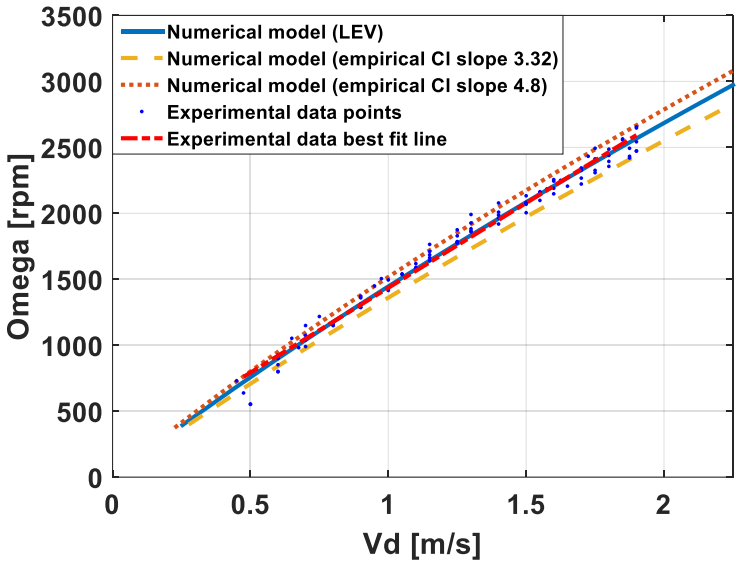

Figure 16: Tuned model results and experimental results (incl. best fit line), with a comparison of the changes on the BEM results when the Cl curves based on Azuma's empirical Cl slopes [19]*. Omega (rpm) = revolutions per minute, Vd = vertical flow speed.*

VI. CONCLUSIONS

An analytical model shown to be capable of modelling the flight of samara seeds was developed, checked, and validated. This was done using Polhamus' leading-edge suction analogy for Leading Edge Vortex (LEV) lift, incorporating it into a Blade Element Model (BEM) to simulate the samara rotor. The model was updated with the coning angle, pitch angle, and flapping rate observed in the experiments, and then the results from the experiments were compared against those from the developed analytical-numerical model, showing extremely good agreement. Saying this however, further validation studies would still be needed, particularly at different settings of blade pitch and coning angles.

With the creation and validation of a numerical model that can predict the rotational speed and vertical rate of descent of falling samara seeds, another step has been taken towards the understanding of LEVs over samara wings, and towards their use in the design of more efficient rotors and/or micro rotary vehicles.

Furture work will focus on enhacing the the experimental setup, and upgrading and validating the the numerical model for defferent parameters.

REFERENCES

[1] S. A. L. Ran Nathan, Gabriel G. Katul, Henry S. Horn, Suvi M. Thomas, Ram Oren, Roni Avissar, Stephen W. Pacala, "Mechanisms of long-distance dispersal of seeds by wind," *Nature*, vol. 418, no. 6896, p. 409, 2002.

[2] D. Lentink, W. B. Dickson, J. L. van Leeuwen, and M. H. Dickinson, "Leading-edge vortices elevate lift of autorotating plant seeds.," *Science*, vol. 324, no. 5933, pp. 1438–40, Jun. 2009.

[3] E. Salcedo, C. Treviño, R. O. Vargas, and L. Martínez-Suástegui, "Stereoscopic particle image velocimetry measurements of the three-dimensional flow field of a descending autorotating mahogany seed (Swietenia macrophylla).," *J. Exp. Biol.*, vol. 216, no. Pt 11, pp. 2017–30, Jun. 2013.

[4] W. Shyy, Y. Lian, J. Tang, D. Viieru, and H. Liu, *Aerodynamics of Low Reynolds Number Flyers*. Cambridge: Cambridge University Press, 2007.

[5] W. Shyy, H. Aono, C. Kang, and H. Lui, *An Introduction to Flapping Wing Aerodynamics*, 1st ed. Cambridge University Press, 2013.

[6] A. L. R. Thomas, G. K. Taylor, R. B. Srygley, R. L. Nudds, and R. J. Bomphrey, "Dragonfly flight: free-flight and tethered flow visualizations reveal a diverse array of unsteady lift-generating mechanisms, controlled primarily via angle of attack.," *J. Exp. Biol.*, vol. 207, no. Pt 24, pp. 4299–323, Nov. 2004.

[7] F. T. Muijres, L. Christoffer Johansson, Y. Winter, and A. Hedenström, "Leading edge vortices in lesser long-nosed bats occurring at slow but not fast flight speeds.," *Bioinspir. Biomim.*, vol. 9, no. 2, p. 025006, Jun. 2014.

[8] I. Gursul, Z. Wang, and E. Vardaki, "Review of flow control mechanisms of leading-edge vortices," *Prog. Aerosp. Sci.*, vol. 43, no. 7–8, pp. 246–270, Oct. 2007.

[9] K. Yasuda and A. Azuma, "The Autorotation Boundary in the Flight of Samaras," *J. Theor. Biol.*, vol. 185, no. 3, pp. 313–320, Apr. 1997.

[10] S. a. Ansari, R. Żbikowski, and K. Knowles, "Aerodynamic modelling of insect-like flapping flight for micro air vehicles," *Prog. Aerosp. Sci.*, vol. 42, no. 2, pp. 129–172, Feb. 2006.

[11] E. C. Polhamus, "A Concept of the Vortex Lift of Sharp-Edge Delta Wings Based on a Leading-Edge-Suction Analogy," *NASA Tech. note*, 1966.

[12] L. W. Traub, "Analysis and Estimation of the Lift Components of Hovering Insects," *J. Aircr.*, vol. 41, no. 2, pp. 284–289, 2004.

[13] M. R. a Nabawy and W. J. Crowther, "On the quasi-steady aerodynamics of normal hovering flight part I: the induced power factor," *J. R. Soc. Interface*, vol. 11, p. 20131196, 2014.

[14] W. J. Maybury, J. M. Rayner, and L. B. Couldrick, "Lift generation by the avian tail.," *Proc. Biol. Sci.*, vol. 268, no. 1475, pp. 1443–8, Jul. 2001.

[15] U. University of Bristol, K. Royal Institute of Technology, L. Linköping University, and R. L. Redhamer Consulting Ldt, "Tornado, the Vortex lattice method." [Online]. Available: http://www.redhammer.se/tornado/. [Accessed: 25-Mar-2015].

[16] "AVL - Aerodynamic and flight-dynamic analysis." [Online]. Available: http://web.mit.edu/drela/Public/web/avl/. [Accessed: 06-May-2016].

[17] J. E. Lamar, "Extension of Leading-Edge-Suction Analogy To Wings With Separated Flow Around The Side Edges At Subsonic Speeds," 1974.

[18] R. G. Bradley, "Vortex-Lift Prediction for Complex Wing Planforms," *J. Aircr.*, vol. 10, no. 6, pp. 379–381, 1973.

[19] A. Azuma and K. Yasuda, "Flight Performance of Rotary Seeds," *J. Theor. Biol.*, no. 138, pp. 23–53, 1989.

[20] S. Joon, L. Eui, J. Lee, and M. Hwan, "Mechanism of autorotation flight of maple samaras (Acer palmatum)," 2014.

[21] E. Limacher and D. E. Rival, "On the distribution of leading-edge vortex circulation in samara-like flight," pp. 316–333, 2015.

[22] P. Bradshaw and R. C. Pankhurst, "The design of low-speed wind tunnels," *Prog. Aerosp. Sci.*, vol. 5, pp. 1–69, 1964.

[23] S. Brusca, R. Lanzafame, and M. Messina, "Low-Speed Wind Tunnel: Design and Build," in *Wind Tunnels: Aerodynamics, Models and Experiments*, 1st ed., J. D. Pereira, Ed. New York: Nova Science Publishers, 2011.

[24] "BitFenix Spectre PRO 230mm - Black | OcUK." [Online]. Available: https://www.overclockers.co.uk/bitfenix-spectre-pro-230mm-black-fg-020-bx.html. [Accessed: 12-Apr-2016].

[25] "Acer pseudoplatanus - Queensland Government." [Online]. Available: http://keyserver.lucidcentral.org/weeds/data/media/Html/acer_pseudoplatanus.htm. [Accessed: 12-Apr-2016].

[26] "Sycamore (Acer pseudoplatanus) - Woodland Trust." [Online]. Available: https://www.woodlandtrust.org.uk/visiting-woods/trees-woods-and-wildlife/british-trees/common-non-native-trees/sycamore/. [Accessed: 12-Apr-2016].

[27] "MiniCTA Measurement System | Dantec Dynamics." [Online]. Available: http://www.dantecdynamics.com/minicta-system. [Accessed: 16-Apr-2016].